Advances in Water Resources 144 (2020) 103703

Contents lists available at ScienceDirect

Advances in Water Resources

journal homepage: www.elsevier.com/locate/advwatres

On proper orthogonal decomposition (POD) based reduced-order modeling of groundwater flow through heterogeneous porous media with point source singularity

Saumava Dey, Anirban Dhar*

Civil Engineering Department, Indian Institute of Technology Kharagpur, Kharagpur, West Bengal, 721302, India

ARTICLE INFO

Keywords:
Random heterogeneity
Finite volume method
Singular point source/sink
Reduced-order model
Proper orthogonal decomposition

ABSTRACT

Groundwater, being a vital component of the natural water resource system, needs continuous monitoring and dynamic management strategies. That said, we require computationally inexpensive groundwater flow models for repetitive solutions with desirable accuracy under budgetary limitation(s). Natural aquifer systems inherit strong heterogeneity at local scales. In this work, we have proposed ordinary kriging-based sequential algorithm for generating replicates of randomly distributed heterogeneous hydraulic conductivity field (Monte Carlo method-based algorithm) conditioned by field values from sampled locations in an irregular-unstructured grid system. Finite Volume method-based groundwater models often encounter difficulties with the representation of point source/sink terms operating within the domain. In this paper, we have proposed an irregular-unstructured grid Finite Volume discretization technique for overcoming the singularity of point source/sink term to yield a consistent output with different grid dimensions. Furthermore, full-system groundwater models often come with a substantial computational burden. Hence, reduction in model order cuts down the computational expenses (in terms of CPU time and usage) to a significant level. We have also put forth a model order reduction methodology for three different illustrative pumping tests. The proposed framework for the model order reduction projects the governing groundwater flow equation onto a set of identified patterns or orthonormal basis functions, applying the Galerkin Projection method to compute a vector of time-dependent coefficients. We have performed pattern identification by Singular Value Decomposition (SVD) of snapshots of full-system model simulation data at selected time instants within the pumping test time domain. The numerical results of the proposed reduced-order models show a good approximation of the full-system models at a comparatively lesser computational time. The accuracy and efficiency of the models attempt to ensure their potential applicability for identifying groundwater dynamics.

1. Introduction

Groundwater management framework requires the repetitive use of groundwater flow models for designing a sustainable policy. With time, scientists have developed several mathematical models to estimate the groundwater dynamics of different aquifer systems. Finite Difference (FD) methods-based models such as MODFLOW (McDonald and Harbaugh, 1988; Harbaugh et al., 2000; Harbaugh, 2005) have wide applications in groundwater modeling. As FD models work on a simple rectangular grid system, the discretization of governing equations is very straightforward. This makes the FD scheme popular among practitioners. However, the FD scheme fails to describe precisely the boundaries of domains with complex geometry, which significantly affects the accuracy of model prediction near the boundaries. Although grid refinement can be a remedy for the incurred loss in accuracy (Mehl and Hill, 2002), it comes at the cost of increased computational expenses. An improved version of the FD scheme, the Integrated Finite Difference (IFD) method also known as the Control Volume Finite Difference (CVFD) method, has been used as well to analyze fluid flow in porous media (Narasimhan and Witherspoon, 1976). MODFLOW-USG (Panday et al., 2013), a CVFD-based unstructured grid version of MODFLOW, has been developed to solve tightly coupled multiple hydrological flow processes. Other numerical methods like Finite Element (FE) method (Reddy, 2006), Boundary Element (BE) method (Kobayashi and Nishimura, 1992), Finite Volume (FV) method (Leveque, 2002; Mazumder, 2016), and different Mesh-free methods (Liu and Gu, 2005) have proved their relevance in modeling groundwater flow over time. Another attractive numerical method for groundwater modeling is the FE method. The FE-based commercial computer models like FEFLOW (Diersch, 2014) and FEMWATER (Lin et al., 1997) are also available for simulation of saturated/unsaturated subsurface flow and transport. Nevertheless, the accuracy of the FE method suffers due to its non-conservative nature. Nowadays, the FV method is gaining acceptance among emerging

* Corresponding author.
E-mail address: anirban@civil.iitkgp.ac.in (A. Dhar).

https://doi.org/10.1016/j.advwatres.2020.103703
Received 20 January 2020; Received in revised form 7 July 2020; Accepted 22 July 2020
Available online 24 July 2020
0309-1708/

numerical methods because it is highly conservative. Moreover, the FV method is also applicable to domains with complex geometries. The FV method integrates the flow-governing equations over the control volume of any shape and conserves the mass, momentum, and the energy entering and exiting a system. FV models for groundwater flow applications have been developed for different regular and irregular-unstructured grid systems (Loudyi et al., 2006; Dotlić et al., 2016).

In groundwater modeling, a well is treated as a singular point source or sink. Moreover, a well encountered in groundwater hydrology, be it of recharging or extraction type, is of vanishingly small radius in the order of 0.1-0.2 metres (Bear, 1979; Pinder and Celia, 2006). The drawdown inside such a small diameter well can be calculated neglecting the water derived from the storage inside the well (Papadopulos and Cooper, 1967). In numerical modeling, a well is specified at the centroid of an element when the governing partial differential equation is discretized on a regular-structured or unstructured grid using FD and CVFD schemes. The problem arises during simulation of real-life situations because the circumference of a well where the pressure gradient is maximum is practically very small compared to the area of the element containing it. Peaceman method defines the well-block pressure in terms of the pressure in the neighbouring elements. It is depicted to be numerically equal to the actual pressure at an effective radius of $0.2\Delta x$ for regular square grid (Peaceman, 1977) and $0.14\left(\Delta x^2 + \Delta y^2\right)^{\frac{1}{2}}$ for regular rectangular grid (Peaceman, 1983) systems. However, local grid refinement around a well can be considered to bring down the effective radius very close to the actual value. On the other hand, finer spatial discretization imposes several restrictions on temporal discretization to maintain stability of the numerical scheme. This eventually increases the computational expenses turning it into an impractical attempt. Furthermore, when irregular-unstructured grid systems are considered, the above considerations do not function as grid dimensions vary for each element, thereby separate well models become a necessity. Different well models for standard FEM, control volume FEM, and mixed FEM have been developed by Chen and Zhang (2009). The well model derived for control volume FEM has been applied for CVFD scheme in MODFLOW-USG (Panday et al., 2013) which is approximately equivalent to Peaceman method applied for structured grids in previous versions of MODFLOW. Regardless, bringing down the effective well radius close to the actual radius value still remains an unanswered question.

The application of any groundwater flow model requires the identification of aquifer parameters such as the hydraulic conductivity field and the storage coefficients. The primary means of aquifer characterization are on-field pumping tests and numerical simulations. As pumping tests are complex and expensive, alternative economical methods based on particle-size distribution (Rogiers et al., 2012) and Electrical Resistivity Tomography (ERT) data (Yu and Wu, 2006) have been used to estimate field hydraulic conductivity. One of the significant challenges faced in modeling groundwater flow through porous media is the mathematical replication of parameter heterogeneity inherent to transport media. Previously, to avoid complexities, the concept of equivalent porous medium was prevalent where the effects of heterogeneity were lumped into a single effective parameter which represented the medium. Yeh (1986) has modeled the field heterogeneity by dividing the flow regime into several sub-regions where a constant hydraulic conductivity characterizes each region. Kriging is an important tool used in groundwater hydrology for distributing field information throughout the domain from limited data points. The kriging estimates are highly influenced by the uncertainty of the semivariogram as it is determined on the basis of available sampled data. The uncertainty of the model semivariogram can be quantified using random fields which is very essential for stochastic modeling (Lin and Chen, 2005). Xu et al. (2017) has shown the successful application of kriging-based interpolation technique to determine spatial distribution of hydraulic conductivity obtained from resistivity and grain-size data at sampled locations.

In reality, aquifer parameters not only vary among different layers, the variation within a particular layer is also of much significance. The heterogeneity of a hydraulic conductivity field is stochastically best described by a log-normal probability density function (Freeze, 1975). A stochastic model of porous media considers hydraulic conductivity as a random variable (Greenkorn and Kessler, 1969), and the intrinsic heterogeneity as a Space Random Function (SRF) correlated in space and time (Bellin and Rubin, 1996). Monte Carlo method-based sequential Gaussian simulation is considered an efficient algorithm for the generation of random fields. Application of the Monte Carlo method to such SRF field generation simplifies the intricacies associated with the replication of spatial variability of field heterogeneity. However, a significant limitation of the Monte Carlo method is that it converges slowly as $\mathcal{O}[\frac{1}{\sqrt{N}}]$ where N is the number of independent Monte Carlo realizations. In order to obtain nearly accurate results, we require a large number of Monte Carlo replicates of the random field, which eventually increases the computation time of the model. Many effective commercial softwares are available for random field generation based on sequential Gaussian simulation. Random Surface Generation (RSG) is a Moving Average method-based software used for generating Gaussian random surfaces to account for the topographic height variations over a surface (Bergström et al., 2007). Similarly, Random Finite Element Method (RFEM) is a FEM-based geotechnical modeling software which generates Gaussian random fields for introducing random behavior of geologic formations (Smith et al., 2013).

On the other hand, exhibiting the characteristics of a hydraulic conductivity field requires the generated field realization to be conditioned by field measurements. Conditional simulation of heterogeneous porous formations based on measured hydraulic conductivity or transmissivity data at few points of the formation have been successfully attempted (Delhomme, 1979; Dagan, 1982; Clifton and Neuman, 1982; Tsai, 2006). TBSIM, a computer program for conditional simulation of Gaussian random fields (Emery and Lantuéjoul, 2006) is also available for simulating random fields conditioned by available data at selected locations. By far, Stanford Geostatistical Modeling Software (SGeMS) (Remy et al., 2009) is the most productive conditional Gaussian random field generator used to generate random fields replicating the properties of heterogeneous porous media. Although the aquifer is intrinsically heterogeneous, in continuum approach to flow through porous media, the parameters are considered to be homogeneous within a small volume known as Representative Elementary Volume (REV) (Bear, 1979; Pinder and Celia, 2006). This implies that natural heterogeneous porous media is homogeneous at microscopic scale. Hence, accurate mathematical formulations should consider a suitable REV for the conditioning data while generating fields that characterize natural geologic formations.

The accuracy of a groundwater model highly depends on the discretization of the spatial and the temporal domain. Finer the discretization, more accurate are the model predictions. This increases the computational expenses making it an inefficient one in the case of high-dimensional models. Therefore, the focus should be on the development of a model that optimizes both the efficiency parameters - accuracy and computation time. Scientists of various genre have acclaimed the model order reduction methodology based on data-driven pattern identification techniques in different fields of scientific study over the past few decades (Sirovich, 1987; Park and Cho, 1996; Park et al., 1999; Haasdonk and Ohlberger, 2011; Hasenauer et al., 2012; Dehghan and Abbaszadeh, 2018; Abbaszadeh and Dehghan, 2020). The method projects the governing equation onto a reduced sub-space of identified patterns, thereby cutting down the number of algebraic equations to be solved for each temporal iteration. Vermeulen et al. (2004) made the first attempt towards low-dimensional modeling of groundwater flow systems. Since then, model reduction technique has been applied to modeling of groundwater flow through both confined (Pasetto et al., 2011; 2013; Boyce and Yeh, 2014) and unconfined aquifers (Boyce et al., 2015; Stanko et al., 2016), groundwater contamination problems

(Ilati and Dehghan, 2016; Kani and Elsheikh, 2019) and groundwater optimization and management studies (McPhee and Yeh, 2008; Baú, 2012). In reduced-order modeling, snapshot selection is the key to pattern recognition. Hence, the temporal distribution of snapshots for groundwater flow systems (Siade et al., 2010) should be chosen wisely. The applications of model order reduction for characterizing aquifer dynamics are limited to FD and FE methods till date. As the FV method is a highly useful tool for PDE discretization, reducing the degrees of freedom involved in the classical approach will help in minimizing the computational complexities.

In this paper, we have presented an FV-based computationally inexpensive mathematical model for evaluating the dynamics of groundwater flow through a heterogeneous confined aquifer subjected to singular point source/sink. In the first step, we have developed a fast, effective and accurate algorithm for generating spatially-correlated and randomly distributed heterogeneous hydraulic conductivity field based on available field values from sampled locations by integrating the concept of REV into standard sequential Gaussian simulation technique. We have developed the field for an irregular-unstructured grid system to facilitate the application of advanced numerical tools. Secondly, we have presented an FV formulation to estimate the groundwater response through the generated random heterogeneous field subjected to singularity of point source/sink. In the proposed methodology, we have considered the actual radius of the well which is independent of the grid dimensions. We have carried out a separate study of the proposed FV-based full-system model through a homogeneous confined aquifer to compare the performance of the model with MODFLOW simulation results. Finally, we have performed POD-based reduced order modeling to minimize the computational expenses in terms of CPU time and usage acquired by the proposed FV-based full-system model.

2. Random heterogeneous field generation technique

In this section, we have introduced an ordinary kriging-based sequential Gaussian simulation technique to generate a random hydraulic conductivity field in an irregular-unstructured grid system. Ordinary kriging is a geostatistical method for interpolating a variable value at any desired location within the domain based on available neighborhood data (Goovaerts, 1997). To integrate the influence of homogeneity at the scale of REV, we have introduced a set of area coefficients along with the set of kriging coefficients used in usual ordinary kriging method. As a result, we have a new non-bias condition which includes both the area coefficients and the kriging coefficients.

2.1. Basis points

In this approach, we have considered a set of basis points whose values have been used for conditioning the estimated values. We have assumed a physical domain, Ω, with field hydraulic conductivity values, K_{α_i}, available at n_1 sampled locations acting as the primary basis points. Initially, we have assigned an influence zone for each sampled location over which we have assumed the corresponding field hydraulic conductivity value to be constant. We have adopted Voronoi tessellation method for the above zonation procedure. The Voronoi polygon area corresponding to i^{th} sampled location is A_{α_i} $(i = 1, \dots, n_1)$. Furthermore, we have overlaid an irregular-unstructured grid system with n_2 elements on the domain Ω. The area of the j^{th} discretized element is denoted by A_{β_j} $(j = 1, \dots, n_2)$, which is considered to be the REV for the hydraulic conductivity value ($K_{\beta_j}{}^*$) estimation at the centroid of the element. The estimates of hydraulic conductivity for these n_2 elements are determined based on the available field values at n_1 basis points as conditioning data. Assuming hydraulic conductivity to vary log normally (Freeze, 1975), we have defined two variables Z_{α_i} and $Z_{\beta_j}{}^*$ as,

$$Z_{\alpha_i} = \ln(K_{\alpha_i}) \qquad i = 1, \dots, n_1 \tag{1}$$

$$Z_{\beta_j}{}^* = \ln(K_{\beta_j}{}^*) \qquad j = 1, \dots, n_2 \tag{2}$$

2.2. Search neighborhood

Here, we have followed an a priori determined random sequential arrangement of the elements for the generation of each Monte Carlo replicate of the hydraulic conductivity field. Such an approach enhances randomness within the generated field. We have considered two different categories of conditioning data: (i) available hydraulic conductivity values from primary basis points; (ii) values from the secondary set of basis points that include elements with previously generated hydraulic conductivity estimates (unavailable for initial estimates). Hence, we have considered two different-sized search neighborhoods for selecting the above two categories of conditioning data (Fig. 1). We have approximated an initial search radius (R_1) for selecting the primary conditioning data as (Isaaks and Srivastava, 1989):

$$R_1 = \sqrt{\frac{\sum_{i=1}^{n_1} A_{\alpha_i}}{n_1}} \tag{3}$$

We have incremented the search radius by ϵ_R as long as a pre-defined number of conditioning data are not selected. However, we have considered the search radius for the second category of conditioning data to be constant for the entire procedure. We have assumed the characteristic length used for irregular-unstructured grid generation as the equivalent search radius (R_2) for the secondary basis points. By this approach, we have attempted to optimize the search neighborhood for computational efficiency without sacrificing the accuracy of the estimates.

2.3. Conditional mean and variance

Let us assume that the neighborhood encloses m_1 primary basis points with corresponding logarithmic values of field hydraulic conductivity, Z_{α_r} (where, $r = 1, \dots, m_1$), and m_2 secondary basis points with previously generated conditional estimates, $Z_{\beta_s}{}^*$ (where, $s = 1, \dots, m_2$), for the k^{th} element. We have generated the conditional estimate of hydraulic conductivity for the k^{th} element from a standard random generator which generates random values following normal distribution with conditional mean (m_c) and conditional variance ($\sigma_c{}^2$) as target statistics (Bellin and Rubin, 1996). We have calculated the conditional mean (m_c) as:

$$m_c = m_{uc} + \sum_{r=1}^{m_1} \phi_{\alpha_r} \lambda_{\alpha_r} [Z_{\alpha_r} - m_{uc\alpha}] + \sum_{s=1}^{m_2} \phi_{\beta_s} \lambda_{\beta_s} [Z_{\beta_s}{}^* - m_{uc\beta}] \tag{4}$$

where, $m_{uc\alpha}$, $m_{uc\beta}$ and m_{uc} respectively, are area-weighted unconditional means based on primary data, secondary data and their combination available within the neighborhood and can be represented as the following:

$$m_{uc\alpha} = \frac{\sum_{r=1}^{m_1} Z_{\alpha_r} A_{\alpha_r}}{\sum_{r=1}^{m_1} A_{\alpha_r}} \tag{5}$$

$$m_{uc\beta} = \frac{\sum_{s=1}^{m_2} Z_{\beta_s}{}^* A_{\beta_s}}{\sum_{s=1}^{m_2} A_{\beta_s}} \tag{6}$$

$$m_{uc} = \frac{\sum_{r=1}^{m_1} Z_{\alpha_r} A_{\alpha_r} + \sum_{s=1}^{m_2} Z_{\beta_s}{}^* A_{\beta_s}}{\sum_{r=1}^{m_1} A_{\alpha_r} + \sum_{s=1}^{m_2} A_{\beta_s}} \tag{7}$$

We have calculated the conditional variance ($\sigma_c{}^2$) as:

$$\sigma_c{}^2 = \sigma_{uc}{}^2 + \sum_{r=1}^{m_1} \phi_{\alpha_r} \lambda_{\alpha_r} \gamma(Z_{\alpha_r}, Z_{\beta_k}{}^*) + \sum_{s=1}^{m_2} \phi_{\beta_s} \lambda_{\beta_s} \gamma(Z_{\beta_s}{}^*, Z_{\beta_k}{}^*) \tag{8}$$

where, $\sigma_{uc}{}^2$ and m respectively are area-weighted unconditional variance and mean calculated based on all available primary data over the entire domain and can be expressed as the following:

$$\sigma_{uc}{}^2 = \frac{\sum_{i=1}^{n_1} A_{\alpha_i} [Z_{\alpha_i} - m]^2}{\sum_{i=1}^{n_1} A_{\alpha_i}} \tag{9}$$

$$m = \frac{\sum_{i=1}^{n_1} A_{\alpha_i} Z_{\alpha_i}}{\sum_{i=1}^{n_1} A_{\alpha_i}} \tag{10}$$

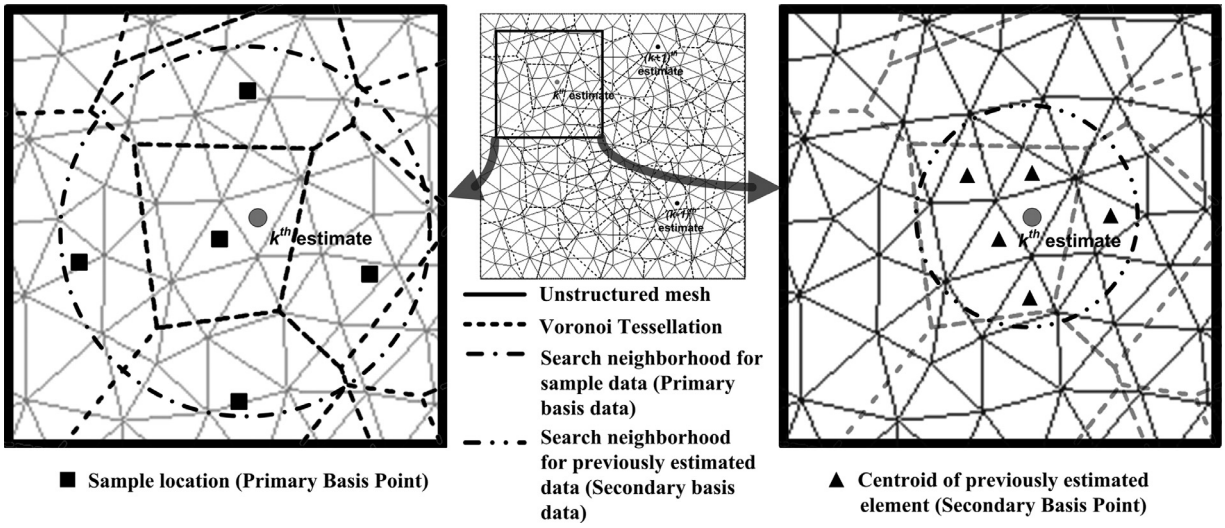

Fig. 1. Schematic diagram showing the selection of primary and secondary conditioning data from the defined neighborhood of an element.

2.4. Area-weighting coefficients

We have introduced a set of area-weighted coefficients ϕ_{α_r} and ϕ_{β_s} which are calculated as:

$$\phi_{\alpha_r} = \frac{A_{\alpha_r}}{\sum_{r=1}^{m_1} A_{\alpha_r}} \qquad r = 1, \ldots, m_1 \tag{11}$$

$$\phi_{\beta_s} = \frac{A_{\beta_s}}{\sum_{s=1}^{m_2} A_{\beta_s}} \qquad s = 1, \ldots, m_2 \tag{12}$$

2.5. Semivariogram model

A continuous function has to be fitted to the experimental semivariogram (Goovaerts, 1997) to calculate the covariance or semivariogram values for any lag distance, h. The best fit function, also known as the 'Model semivariogram', is used for the kriging method. We have selected an unbounded semivariogram with power-law dependence of variance, γ, on lag distance h:

$$\gamma(|h|) = c|h|^{\omega} \tag{13}$$

We can consider a porous medium as a distribution of interconnected channels with random obstructions at different length-scales between them. Fractal geometry is an emerging mathematical tool for studying the behavior of irregular geometric objects and has been successfully applied to porous geological formations to determine its fractal nature (Adler and Thovert, 1993). Moreover, the application of fractal geometry at the micro-scale level has also simplified the problems of spatial heterogeneity characterization of porous media and transport phenomenon through the same (Sahimi and Yortsos, 1990). A self-similar fractal field requires the correlation of the hydraulic conductivity values over greater lengths, and this unbounded power-law semivariogram model (13) stands out as the appropriate choice. Furthermore, for $\omega > 1$, the field shows smooth variation and looks highly realistic.

2.6. Determination of Kriging coefficients

We can express the error variance for conditional estimation of hydraulic conductivity for the k^{th} element as:

$$\sigma_{error}{}^2 = Var[Z_{\beta_k}{}^* - Z_{\beta_k}] = Var[Z_{\beta_k}{}^*] + Var[Z_{\beta_k}] - 2Cov[Z_{\beta_k}{}^*, Z_{\beta_k}]$$
$$= \sum_{r=1}^{m_1}\sum_{s=1}^{m_1} \phi_{\alpha_r}\lambda_{\alpha_r}\phi_{\alpha_s}\lambda_{\alpha_s} C_z(Z_{\alpha_r}, Z_{\alpha_s}) + \sum_{r=1}^{m_1}\sum_{s=1}^{m_2} \phi_{\alpha_r}\lambda_{\alpha_r}\phi_{\beta_s}\lambda_{\beta_s} C_z(Z_{\alpha_r}, Z_{\beta_s}{}^*)$$
$$+ \sum_{r=1}^{m_2}\sum_{s=1}^{m_1} \phi_{\beta_r}\lambda_{\beta_r}\phi_{\alpha_s}\lambda_{\alpha_s} C_z(Z_{\beta_r}{}^*, Z_{\alpha_s}) + \sum_{r=1}^{m_2}\sum_{s=1}^{m_2} \phi_{\beta_r}\lambda_{\beta_r}\phi_{\beta_s}\lambda_{\beta_s} C_z(Z_{\beta_r}{}^*, Z_{\beta_s}{}^*)$$
$$+ C_z(0) - 2\sum_{r=1}^{m_1} \phi_{\alpha_r}\lambda_{\alpha_r} C_z(Z_{\alpha_r}, Z_{\beta_k}) - 2\sum_{s=1}^{m_2} \phi_{\beta_s}\lambda_{\beta_s} C_z(Z_{\beta_s}{}^*, Z_{\beta_k}) \tag{14}$$

Ordinary kriging produces estimates with minimum estimation error variance. For constraining the minimization problem, we have defined the non-bias condition comprising the kriging and area coefficients for both the primary and secondary data as the following:

$$\sum_{r=1}^{m_1} \phi_{\alpha_r}\lambda_{\alpha_r} + \sum_{s=1}^{m_2} \phi_{\beta_s}\lambda_{\beta_s} = 1 \tag{15}$$

Here, we have introduced a Lagrange multiplier μ for converting the constrained minimization problem into an unconstrained one, and have defined a new function for error variance as:

$$L = \sigma_{error}{}^2 + 2\mu\left[\sum_{r=1}^{m_1} \phi_{\alpha_r}\lambda_{\alpha_r} + \sum_{s=1}^{m_2} \phi_{\beta_s}\lambda_{\beta_s} - 1\right] \tag{16}$$

The minimization of the new error variance function yields a set of $(m_1 + m_2)$ linear algebraic equations. The set of first m_1 equations obtained from the condition $\frac{\partial L}{\partial \lambda_{\alpha_r}} = 0$ is as follows:

$$\sum_{s=1}^{m_1} \phi_{\alpha_s}\lambda_{\alpha_s}\gamma(Z_{\alpha_p}, Z_{\alpha_s}) + \sum_{s=1}^{m_2} \phi_{\beta_s}\lambda_{\beta_s}\gamma(Z_{\alpha_p}, Z_{\beta_s}{}^*) - \mu = \gamma(Z_{\alpha_p}, Z_{\beta_k})$$
$$\text{for } p = 1, \ldots, m_1 \tag{17}$$

The next set of m_2 equations obtained from the condition $\frac{\partial L}{\partial \lambda_{\beta_r}} = 0$ is as follows:

$$\sum_{s=1}^{m_1} \phi_{\alpha_s}\lambda_{\alpha_s}\gamma(Z_{\beta_q}{}^*, Z_{\alpha_s}) + \sum_{s=1}^{m_2} \phi_{\beta_s}\lambda_{\beta_s}\gamma(Z_{\beta_q}{}^*, Z_{\beta_s}{}^*) - \mu = \gamma(Z_{\beta_q}{}^*, Z_{\beta_k})$$
$$\text{for } q = 1, \ldots, m_2 \tag{18}$$

The ordinary kriging coefficients and the Lagrange multiplier (μ) have been calculated by simultaneously solving the set of $(m_1 + m_2)$ equations [(17) and (18)] and the non-bias condition (15). As the spatial configuration of the conditioning data for any element is not constant for an irregular-unstructured grid system, we need to compute the ordinary kriging coefficients repeatedly for every element.

3. Governing equation

The transient saturated groundwater flow through a heterogeneous and isotropic confined aquifer with extraction is governed by

(Bear, 1979):

$$S_s \frac{\partial s_a(\mathbf{x},t)}{\partial t} - \nabla \cdot [\mathbf{K} \nabla s_a(\mathbf{x},t)] + W_s + \sum_i N_s(\mathbf{x},t)\delta(\mathbf{x}-\mathbf{x_i},t) = 0 \tag{19}$$

$\mathbf{x} \in \Omega$

$t \in [0, T_{final}]$

$s_a(\mathbf{x},t) = H_0 - z_a(\mathbf{x},t)$

We have considered the extraction well to be fully penetrating to ensure horizontal flow and constant extraction rate throughout the time domain. As we have ensured the flow to be horizontal, we have defined depth-averaged drawdown in the governing equation, Eq. (19), thereby reducing the flow in two-dimensional space. The governing equation is subjected to the following initial and boundary conditions:

- Initial Condition:

$$s_a(\mathbf{x},0) = s_{a0}(\mathbf{x}) \tag{20}$$

- Dirichlet Boundary Condition:

$$s_a(\mathbf{x},t) = s_{aD}(\mathbf{x},t) \tag{21}$$

$\mathbf{x} \in \Gamma_D \subset \partial\Omega$

- Neumann Boundary Condition:

$$-\mathbf{K}\nabla s_a(\mathbf{x},t).\hat{\mathbf{n}} = q_N(\mathbf{x},t) \tag{22}$$

$\mathbf{x} \in \Gamma_N \subset \partial\Omega$

where,

$$\mathbf{K} = \begin{bmatrix} K_x & 0 \\ 0 & K_y \end{bmatrix}$$

4. Finite volume discretization

The CVFD scheme used in MODFLOW-USG (Panday et al., 2013) has a geometric constraint that the line joining the centroids of the two adjacent elements has to perpendicularly bisect the common face (Narasimhan and Witherspoon, 1976). This geometric requirement is satisfied by grids composed of equilateral triangles, rectangles or other regular higher order polygons, and unstructured grids formed by Voronoi tessellation. While dealing with real-life problems, the grids generated do not always conform to the CVFD criteria, and subsequent error creeps into the solution. In order to reduce the error, the Ghost Node Correction (GNC) package is implemented in MODFLOW-USG, which eventually increases the computation time. However, the FV method completely overcomes this potential source of error arising due to the geometry of the discretized elements by considering a tangential flux term. A tangential flux is generated whenever a line joining the centroids of two adjacent elements is not a perpendicular bisector of their common face. Hence, we have preferred this approach because of its flexibility and mass conservative nature.

In this section, we have illustrated an FV discretization approach for the governing partial differential equation of confined groundwater flow. In this approach, we have considered the singular point source/sink terms separately for their respective operating nodes. The integration of (19) without the point source/sink term over the volume of an element (V_β) and time step (Δt) and subsequent application of Gauss divergence theorem yields:

$$\int_t^{t+\Delta t}\int_{V_\beta} S_s \frac{\partial s_a}{\partial t}\, dV\, dt - \int_t^{t+\Delta t}\int_{A_f} [\mathbf{K}\nabla s_a]\cdot \hat{\mathbf{n}}\, dA\, dt = -\int_t^{t+\Delta t}\int_{V_\beta} W_s\, dV\, dt \tag{23}$$

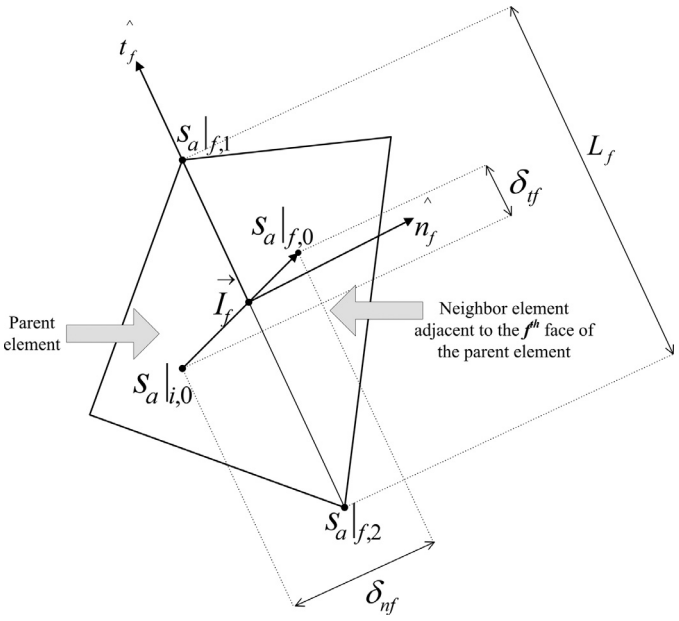

Fig. 2. Schematic diagram of an irregular-unstructured parent element and one of its neighbor element.

Discretization of Eq. (23) for a triangular element in an irregular-unstructured grid produces the following:

$$SA_{\beta_i}\frac{[s_a|_{i,0}{}^{k+1} - s_a|_{i,0}{}^{k}]}{\Delta t} = \sum_{f=1}^{3} T_f\left[(\nabla s_a)_f \cdot \hat{\mathbf{n}}_\mathbf{f}\right]L_f - W_s A_{\beta_i} b \tag{24}$$

where,

$S = S_s\, b$

$T_f = K_f\, b$

We have used the superscript for representing the time-level of the temporal discretization, and the subscript 0 to designate the element-centered values of a variable.

4.1. Gradient approximatio

The gradient term $(\nabla s_a)_f$ at the face f can be decomposed into two components from the point of intersection of the line joining the centroids of the parent and the adjacent neighbor element, one normally outward to the face and the other tangentially along the face (Fig. 2).

$$(\nabla s_a)_f = [(\nabla s_a)_f \cdot \hat{\mathbf{n}}_\mathbf{f}]\hat{\mathbf{n}}_\mathbf{f} + [(\nabla s_a)_f \cdot \hat{\mathbf{t}}_\mathbf{f}]\hat{\mathbf{t}}_\mathbf{f} \tag{25}$$

A dot product of Eq. (25) with the vector $\mathbf{I_f}$ and subsequent rearrangement of the terms yields the following:

$$(\nabla s_a)_f \cdot \hat{\mathbf{n}}_\mathbf{f} = \frac{(\nabla s_a)_f \cdot \mathbf{I_f}}{\delta_{nf}} - \frac{[(\nabla s_a)_f \cdot \hat{\mathbf{t}}_\mathbf{f}]\delta_{tf}}{\delta_{nf}} \tag{26}$$

After performing the dot products of the gradient term $(\nabla s_a)_f$ with $\mathbf{I_f}$ and $\hat{\mathbf{t}}_\mathbf{f}$ in Eq. (26), the final approximation of the gradient term becomes:

$$(\nabla s_a)_f \cdot \hat{\mathbf{n}}_\mathbf{f} = \frac{s_a|_{f,0} - s_a|_{i,0}}{\delta_{nf}} - \left(\frac{s_a|_{f,1} - s_a|_{f,2}}{L_f \delta_{nf}}\right)\delta_{tf} \tag{27}$$

We have used the subscripts 1 and 2 for implying the values at the two nodes of the face f, that distinguish the nodal values from the element-centered values designated by the subscript 0.

4.2. Face-centered approximation of hydraulic conductivity

The FV formulation of groundwater flow in an irregular-unstructured grid system requires an interpolation of the face-centered hydraulic conductivity from adjacent element-centered values. We have performed inverse distance-weighted interpolation for determining the face-centered hydraulic conductivity because it is second order accurate and has certain advantages over other methods (Mazumder, 2016). We can write the interpolation equation as the following:

$$K_f = w_f K|_{i,0} + (1 - w_f) K|_{f,0} \tag{28}$$

where,

$$w_f = \frac{\frac{1}{d_1}}{\frac{1}{d_1} + \frac{1}{d_2}} \tag{29}$$

4.3. Interpolation of element-centered values to Nodal values

Post-processing of the FV algorithm needs an interpolation of nodal values from the calculated element-centered values. We have computed the nodal values using area-weighted interpolation as:

$$s_a|_{f,n} = \sum_{i=1}^{n_p} w_n|_{i,n} s_a|_{i,0} \tag{30}$$

where,

$$w_n|_{i,n} = \frac{A_{\beta_i}}{\sum_{i=1}^{n_p} A_{\beta_i}} \tag{31}$$

4.4. Discretization for all internal elements

We have deduced the FV discretized form of the governing equation for all internal elements as:

$$\begin{aligned} SA_{\beta_i} \frac{[s_a|_{i,0}{}^{k+1} - s_a|_{i,0}{}^{k}]}{\Delta t} &= \sum_{f=1}^{3} T_f \left[\frac{s_a|_{f,0} - s_a|_{i,0}}{\delta_{nf}} - \left(\frac{s_a|_{f,1} - s_a|_{f,2}}{L_f \delta_{nf}} \right) \delta_{tf} \right] L_f \\ &\quad - W_s A_{\beta_i} b \\ &= \sum_{f=1}^{3} \frac{T_f L_f}{\delta_{nf}} [s_a|_{f,0} - s_a|_{i,0}] - \underbrace{\sum_{f=1}^{3} \frac{T_f \delta_{tf}}{\delta_{nf}} [s_a|_{f,1} - s_a|_{f,2}]}_{tangential\ flux} \\ &\quad - W_s A_{\beta_i} b \end{aligned} \tag{32}$$

In the equation above (32), we cannot calculate the tangential flux term directly. Therefore, further approximation is needed. Interpolating the drawdown at each node from the drawdowns of all the associated elements by Eq. (30), we have expanded the tangential flux term as:

$$\begin{aligned} \sum_{f=1}^{3} \frac{T_f \delta_{tf}}{\delta_{nf}} [s_a|_{f,1} - s_a|_{f,2}] &= \left[\frac{T_2 \delta_{t2}}{\delta_{n2}} - \frac{T_3 \delta_{t3}}{\delta_{n3}} \right] \underbrace{\sum_{l_1=1}^{n_{e1}} s_a|_{l_1,0}\, w_n|_{l_1,1}}_{s_a|_{i,1}} \\ + \left[\frac{T_3 \delta_{t3}}{\delta_{n3}} - \frac{T_1 \delta_{t1}}{\delta_{n1}} \right] \underbrace{\sum_{l_2=1}^{n_{e2}} s_a|_{l_2,0}\, w_n|_{l_2,2}}_{s_a|_{i,2}} &+ \left[\frac{T_1 \delta_{t1}}{\delta_{n1}} - \frac{T_2 \delta_{t2}}{\delta_{n2}} \right] \underbrace{\sum_{l_3=1}^{n_{e3}} s_a|_{l_3,0}\, w_n|_{l_3,3}}_{s_a|_{i,3}} \end{aligned} \tag{33}$$

Applying θ-scheme for temporal discretization, we can write the final approximation of Eq. (32) as:

$$a_i\, s_a|_{i,0}{}^{k+1} + \sum_{f=1}^{3} b_{i,f}\, s_a|_{f,0}{}^{k+1} + \sum_{m=1}^{3} d_{i,l_m} \sum_{l_m=1}^{n_{em}} s_a|_{l_m,0}{}^{k+1} w_n|_{l_m,m} = f_i \tag{34}$$

where,

$$a_i = SA_{\beta_i} + \theta \Delta t \sum_{f=1}^{3} \frac{T_f L_f}{\delta_{nf}}$$

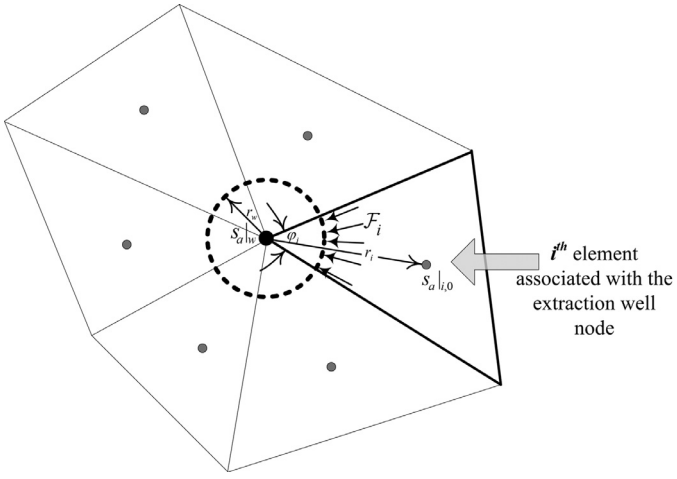

Fig. 3. Schematic diagram of a extraction well node and its associated elements.

$$b_{i,f} = -\theta \Delta t \frac{T_f L_f}{\delta_{nf}} \qquad \text{for } f = 1, 2, 3$$

$$d_{i,l_1} = \theta \Delta t \left[\frac{T_2 \delta_{t2}}{\delta_{n2}} - \frac{T_3 \delta_{t3}}{\delta_{n3}} \right]$$

$$d_{i,l_2} = \theta \Delta t \left[\frac{T_3 \delta_{t3}}{\delta_{n3}} - \frac{T_1 \delta_{t1}}{\delta_{n1}} \right]$$

$$d_{i,l_3} = \theta \Delta t \left[\frac{T_1 \delta_{t1}}{\delta_{n1}} - \frac{T_2 \delta_{t2}}{\delta_{n2}} \right]$$

$$\begin{aligned} f_i = &\left[\frac{SA_{\beta_i}}{\theta} + \left(1 - \frac{1}{\theta}\right) a_i \right] s_a|_{i,0}{}^{k} \\ &+ \left(1 - \frac{1}{\theta}\right) \left\{ \sum_{f=1}^{3} b_{i,f}\, s_a|_{f,0}{}^{k} + \sum_{m=1}^{3} d_{i,l_m} \sum_{l_m=1}^{n_{em}} s_a|_{l_m,0}{}^{k} w_n|_{l_m,m} \right\} \\ &- W_s A_{\beta_i} b \Delta t \end{aligned}$$

4.5. Discretization for extraction well node

In this work, we have presented a generalized FV scheme for confined groundwater flow with singular point source/sink in an irregular-unstructured grid system. Here, we have specified the wells at the nodes in the grid system. An important aspect considered in this formulation is the selection of actual well radius for the calculation of drawdown at the well node, and not the effective radius calculated by any well model. This ensures that the well radius is independent of the grid dimension unlike in MODFLOW-USG where it is dependent on grid dimensions. A linear aquifer-loss coefficient which accounts for the head loss in the well node due to the differences in actual and effective well radius has been applied for multi-node wells in MODFLOW-USG. However, single-node wells simulated by the basic well (WEL) package lacks this correction. Hence, the selection of actual well radius rules out the issues of grid-convergence that may arise with changing grid dimensions. Assuming the flow to be radial in the neighbourhood of a well, the drawdown at a well is calculated by solving the continuity equation at that well node for every time-step. The radially inward flow from the centroids of all the elements associated with the well node are equated with the extraction rate. We have calculated the inward flux through the arc subtended by the well for each element associated with the well node (Fig. 3) as (Thiem, 1906):

$$\mathcal{F}_i = \frac{\varphi_i T|_{i,0} (s_a|_w - s_a|_{i,0})}{\ln \frac{r_i}{r_w}} \tag{35}$$

We can present the continuity equation at the extraction well node as follows:

$$\sum_{i=1}^{n_p} F_i + Q_p = 0 \tag{36}$$

On substituting Eq. (35) in Eq. (36) and rearranging the terms, we get:

$$\sum_{i=1}^{n_p} \frac{\varphi_i T|_{i,0}}{\ln \frac{r_i}{r_w}} {s_a|_w}^{k+1} - \sum_{i=1}^{n_p} \frac{\varphi_i T|_{i,0}}{\ln \frac{r_i}{r_w}} {s_a|_{i,0}}^{k+1} + Q_p = 0 \tag{37}$$

4.6. Discretization for elements associated with the extraction well node

The elements associated with the extraction well node have an additional flux term directed radially towards the node. The final discretized form, after applying the θ-scheme for temporal averaging is as the following:

$$a_i{}^p {s_a|_{i,0}}^{k+1} + \sum_{f=1}^{3} b_{i,f}{}^p {s_a|_{f,0}}^{k+1} + c_i{}^p {s_a|_w}^{k+1} + \sum_{m=1}^{3} {d_{i,l_m}}^p \sum_{l_m=1}^{n_{em}} {s_a|_{l_m,0}}^{k+1} {w_n|_{l_m,m}} = {f_i}^p \tag{38}$$

where,

$$a_i{}^p = a_i + \theta \Delta t \frac{\varphi_i T|_{i,0}}{\ln \frac{r_i}{r_w}}$$

$$c_i{}^p = -\theta \Delta t \frac{\varphi_i T|_{i,0}}{\ln \frac{r_i}{r_w}}$$

$$f_i{}^p = f_i + \left(1 - \frac{1}{\theta}\right) c_i{}^p {s_a|_w}^k$$

However, the coefficients ${b_{i,f}}^p$, ${d_{i,l_1}}^p$, ${d_{i,l_2}}^p$ and ${d_{i,l_3}}^p$ are respectively equal to $b_{i,f}$, d_{i,l_1}, d_{i,l_2} and d_{i,l_3} from Eq. (34).

4.7. Boundary conditions

In groundwater flow problems, we come across three types of boundary conditions: Dirichlet or specified head boundary condition, Neumann or specified flux boundary condition, and Cauchy boundary condition. In the Dirichlet boundary, the hydraulic head is either constant or specified as a function of space and time. For each Dirichlet boundary element, we need to specify the heads for the two nodes lying on the boundary. However, for a Neumann boundary element, the normal flux through the face(s) coinciding with the boundary is/are specified. An impermeable boundary is a particular case of Neumann boundary condition where the specified normal flux through the boundary face is zero. Moreover, the Cauchy boundary condition can be considered as an imposition of both Dirichlet and Neumann conditions on the boundary elements. The FV discretization equations for the elements associated with both Dirichlet and Neumann boundaries are presented in the Supplementary Information (Appendix: SA1).

5. Reduced-Order modeling

Model order reduction is a computationally efficient technique used for solving any full-scale model. In this section, we have presented a reduced-order groundwater flow model applying the standard POD formulation. Since FV method is highly conservative in nature, application of POD to the proposed FV formulation of groundwater flow equation through heterogeneous porous media is expected to yield extremely satisfactory results. The reduced-order model approximates the state variable as the product of an orthogonal matrix $\mathbf{P}(\mathbf{x})$ and a time-dependent coefficient vector $\mathbf{r_n}(t)$ as:

$$\hat{\mathbf{s_a}}(\mathbf{x}, t) = \mathbf{P}(\mathbf{x})\, \mathbf{r_n}(t) \tag{39}$$

5.1. Snapshot selection

Model order reduction methodology starts with a collection of scenarios known as snapshots that tend to describe the dynamics of the system with time. A snapshot matrix stores the solutions of a full-system groundwater model at some pre-defined time instants. We require a careful study of the nature of the governing equation and the evolution of its solution with time for determining the 'snapshot time-set'. For groundwater flow problems, we have selected the 'snapshot time-set' by the following exponential function:

$$\tilde{t}_{si} = \begin{cases} 0 & i = 1 \\ 1 - \tanh\left(\tilde{T}_s(1 - u_i)\right) & \text{otherwise} \end{cases} \tag{40}$$

where,

$$u_i = \frac{i-1}{(n_{\tilde{t}_s} - 1)}$$

The snapshot matrix S_{snap} has been formed from the solutions of Eq. (19) for different time instants given by the time-set $\tilde{\mathbf{t}}_\mathbf{s}$. The required number of sets of snapshots depends on the number of linearly independent constant or variable forcing agent (extraction well) operative within the domain. If multiple forcing agents are present, a single set of snapshots has to be collected separately for each of them. Each set should have the solutions of the model with one forcing agent operative at a constant rate while others are remaining completely inoperative. We have represented the complete snapshot matrix as:

$$\mathbf{S_{snap}}^j = \left[\mathbf{s_a}|_{\tilde{t}_{s1}}, \mathbf{s_a}|_{\tilde{t}_{s2}}, \mathbf{s_a}|_{\tilde{t}_{s3}}, \ldots, \mathbf{s_a}|_{\tilde{t}_{sn_{\tilde{t}_s}}}\right] \qquad \forall j = 1, 2, 3, \ldots, n_{set}$$

$$\mathbf{S_{snap}} = \left[\mathbf{S_{snap}}^1, \mathbf{S_{snap}}^2, \mathbf{S_{snap}}^3, \ldots, \mathbf{S_{snap}}^{n_{set}}\right] \tag{41}$$

5.2. Formation of the POD basis

For orthonormalization of the above snapshot matrix, we have performed Singular Value Decomposition (SVD) of $\mathbf{S_{snap}}$ as:

$$\mathbf{S_{snap}} = \mathbf{U}\mathbf{\Sigma}\mathbf{V}^T \tag{42}$$

After SVD, the matrix $\mathbf{U}$ containing the left singular vectors of $\mathbf{S_{snap}}$ represents the orthogonal matrix $\mathbf{P}(\mathbf{x})$ from Eq. (39), also known as the POD basis. Accordingly, we can call the left singular vectors as the POD basis vectors. Among all POD basis vectors, only a few contributes significantly to maximum information regarding system dynamics. We have chosen the basis vectors corresponding to the singular values satisfying the following relationship for the construction of the final POD basis.

$$\frac{\sum_{i=1}^{\tilde{n}_p} \sigma_i}{\sum_{i=1}^{Rank(\mathbf{S_{snap}})} \sigma_i} \times 100\% \geq 99.99\% \tag{43}$$

5.3. Galerkin projection

We have denoted the matrix form of the discretized governing Eq. (24) as:

$$\mathbf{A}\, \mathbf{s_a} = \mathbf{f} \tag{44}$$

We have split the above equation into two parts, whereby we have separated the extraction well nodes from the elements. We can write the partitioned equation as:

$$\left[\begin{array}{c|c} \mathbf{A_e} & \mathbf{a_p}^T \\ \hline \mathbf{a_p} & \mathbf{A_p} \end{array}\right] \left(\begin{array}{c} \mathbf{s_{ae}} \\ \hline \mathbf{s_{ap}} \end{array}\right) = \left(\begin{array}{c} \mathbf{f_e} \\ \hline \mathbf{f_p} \end{array}\right)$$

$$\mathbf{A_e}\mathbf{s_{ae}} + \mathbf{a_p}^T \mathbf{s_{ap}} = \mathbf{f_e} \tag{45}$$

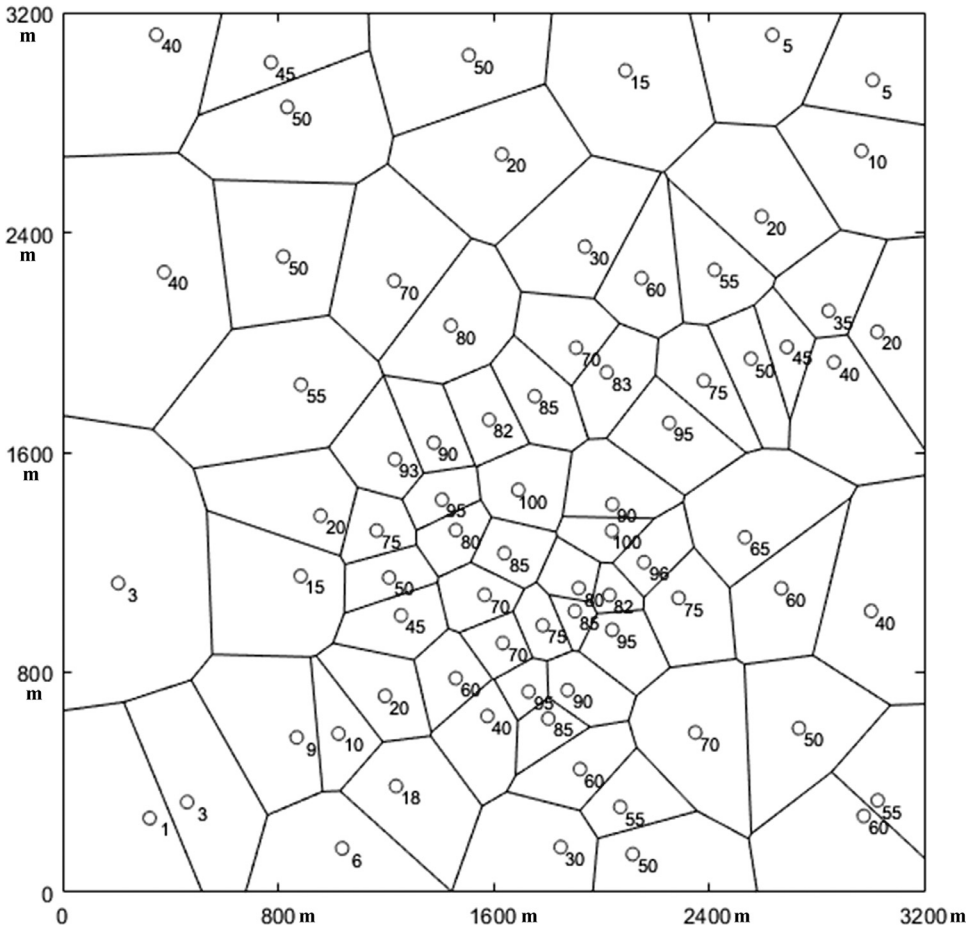

Fig. 4. Voronoi tessellation of the domain with 75 sample locations and corresponding field hydraulic conductivities in *m/day*.

$$\mathbf{a_p s_{ae}} + \mathbf{A_p s_{ap}} = \mathbf{f_p} \tag{46}$$

The Eq. (45) corresponds to the drawdowns at the elements. We have solved this equation by projecting it onto a reduced sub-space of POD basis via Galerkin projection. However, we have calculated the drawdown at the extraction well nodes by solving Eq. (46) explicitly for each time step. In order to initiate the iteration, we have assumed the full-system solution at a very early time-step (in the range of 10^{-5}) as the initial guess vector. The Galerkin Projection of Eq. (45) has been performed by substituting Eq. (39) to form the following:

$$\mathbf{A_e\, Pr_n} = \mathbf{f_e} - \mathbf{a_p}^T\mathbf{s_{ap}}$$

$$\mathbf{P}^T\mathbf{A_e\, Pr_n} = \mathbf{P}^T(\mathbf{f_e} - \mathbf{a_p}^T\mathbf{s_{ap}})$$

$$\mathbf{r_n} = [\mathbf{P}^T\mathbf{AP}]^{-1}[\mathbf{P}^T(\mathbf{f_e} - \mathbf{a_p}^T\mathbf{s_{ap}})] \tag{47}$$

The resulting vector $\mathbf{r_n}$ has been substituted in Eq. (39) to obtain the reduced-order solution at the element centroids. We have then substituted the solution vector $\mathbf{s_{ae}}$ in Eq. (46) to estimate the drawdown at the extraction well locations at the end of each time-step.

6. Numerical tests

6.1. TC1: Random hydraulic conductivity field generation

In order to demonstrate the applicability of the heterogeneous field generation algorithm proposed in Section 2, we have utilized a two-dimensional synthetic square-shaped confined aquifer with sides 3200 m and depth 50 m (Tsai, 2006). We have considered the specific storage coefficient of the aquifer to be $10^{-4}/m$. In order to condition the estimates of hydraulic conductivity, we have obtained field values from 75 sampled locations within the aquifer. Fig. 4 shows the 75 sample locations with respective field hydraulic conductivity values and their corresponding zones formed after Voronoi tessellation. We have computed the experimental semivariogram with these measured field conductivities, and have fitted a power-law model semivariogram (Eq. (13)) with parameters: $c = 10^{-4}$ and $\omega = 1.2462$. We have then discretized the aquifer into 2398 nodes with 5690 triangular elements. We have evaluated the estimates of hydraulic conductivity for these triangular elements by Algorithm 1 with the following input parameters: $N_{c\min} = 5$; $m_{1\max} = 5$; $m_{2\max} = 5$; $\epsilon_R = 100\,m$; and $R_2 = 70\,m$. For each field replicate, the initial estimates have entirely been conditioned by primary basis data searched over large neighborhoods due to the unavailability of secondary basis data. Such estimates are thus bound to be very rough ones. However, the random sequence adopted for the estimation of each field realization ensures smoothening of these rough estimates when a large number of replicates are generated. The effects of local integration over discretization have been insignificant as the correlation length for the unbounded power-law semivariogram is very large compared to the characteristic length used for grid generation (Ababou, 1988). We have displayed the contour diagram of the mean log hydraulic conductivity field averaged over 10^4 Monte Carlo simulations in Fig. 5a. The contour plot of estimation error variance (Fig. 5b) shows minimum variance around the central region of the aquifer, where the primary conditioning data was available in abundance. The maximum error variance is in the range of 0.05 to 0.07, and is observed along the left boundary and near the bottom right boundary - where the density of available primary basis points was the least.

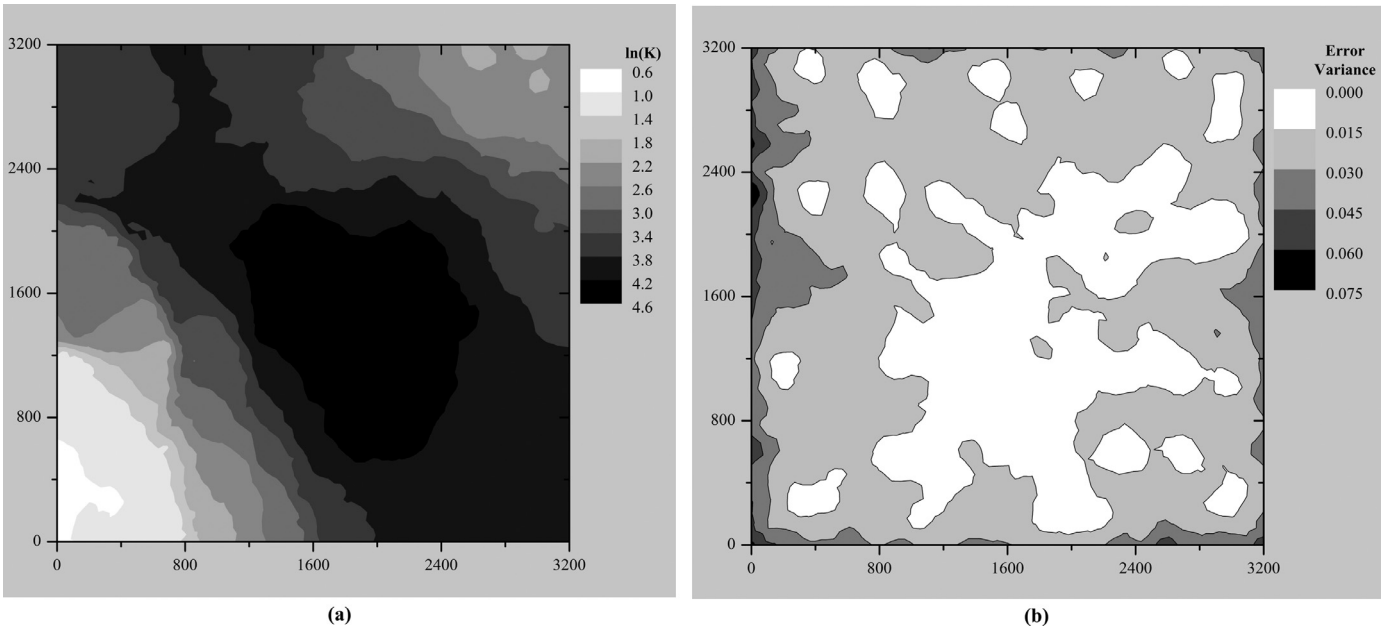

Fig. 5. Contour diagram of (a) estimated ln (K) distribution and (b) estimation error variance.

Algorithm 1: Random Heterogeneous Field Generation.

Input: c, ω, M_c, n_1, n_2, $N_{c\min}$, $m_{1\max}$, $m_{2\max}$, ϵ_R, R_2
Output: ${K_\beta}^*$
Data: A_α, A_β

Compute m [Equation (10)] and ${\sigma_{uc}}^2$ [Equation (9)]
Initialize R_1 [Equation (3)]
for $i = 1 \rightarrow M_c$ **do**
  for $j = 1 \rightarrow n_2$ **do**
    Generate a random number (N_r) between 1 and n_2 (except the number generated in the previous iteration)
    while $(m_1 + m_2) \leq N_{c\min}$ **do**
      Search for primary and secondary basis points within the radius of R_1 and R_2 respectively from the centroid of ${N_r}^{th}$ element
      $R_1 \leftarrow R_1 + \epsilon_R$
    Sort the primary (m_1) and secondary (m_2) basis points in ascending order of their distances from the centroid of ${N_r}^{th}$ element
    if $m_1 \geq m_{1\max}$ **then**
      $m_1 \leftarrow m_{1\max}$
    else
      $m_1 \leftarrow m_1$
    if $m_2 \geq m_{2\max}$ **then**
      $m_2 \leftarrow m_{2\max}$
    else
      $m_2 \leftarrow m_2$
    Compute ϕ_{α_r} (for $r = 1, \ldots, m_1$) [Equation (11)] and ϕ_{β_s} (for $s = 1, \ldots, m_2$) [Equation (12)]
    Solve Equations (15), (17) and (18) for λ_{α_r} (for $r = 1, \ldots, m_1$), λ_{β_r} (for $r = 1, \ldots, m_2$) and μ
    Compute m_c [Equation (4)] and ${\sigma_c}^2$ [Equation (8)]
    Generate a random value ${Z_{\beta_j}}^*$ from the Normal distribution: ${Z_{\beta_j}}^* \sim N(m_c, {\sigma_c}^2)$
    ${K_{\beta_j}}^* \leftarrow e^{{Z_{\beta_j}}^*}$

6.2. TC2: *Transient groundwater flow model with a single extraction well in a homogeneous confined aquifer*

We have tested the FV formulation of the full-system groundwater model and the proposed reduced-order model on the synthetic confined aquifer described in *TC*1. We have assumed the aquifer to be homogeneous with a constant value of hydraulic conductivity 50 m/day throughout the entire domain. We have considered zero Dirichlet boundary conditions on all the boundaries of the confined aquifer. An extraction well extracting at a constant rate of $10^4\, m^3/day$ is located at the center of the aquifer. We have discretized the aquifer into 2851 nodes with 5516 triangular elements. We have performed a pumping test of 15 *days* duration. We have assumed a small-diameter well of radius 0.1 m for all the test problems. We have observed the system to achieve steady-state conditions after 5 *days* of extraction from the drawdowns recorded (Figure SF2b) at three different locations within the aquifer (Figure SF2a).

We have compared the performance of our proposed FV-based full-system model (FSM) with the results of MODFLOW-USG simulations for *TC*2. We have carried out the simulations on a square-grid system in MODFLOW-USG using different grid dimensions. We have used the well (WEL) package for carrying out the simulations. We have observed that the drawdown at the well location is inconsistent with changing grid dimensions. This can be attributed to the fact that the effective well radius considered in the calculation changes with varying grid dimensions. We have applied grid refinement around the well using MODFLOW-LGR so that the effective well radius approaches toward the actual well radius. However, the grid refinement operates at the expense of CPU computation time. The results of our proposed FV-based FSM closely agrees with MODFLOW-USG when the effective well radius is almost equal to the actual well radius. Fig. 6 claims that our proposed FV-based FSM offers better grid-convergence than MODFLOW-USG using the well (WEL) package. The drawdown calculated at the well location for different grid dimensions using MODFLOW-USG and proposed FV-based FSM are tabulated in Table 1 along with the respective CPU computation times.

Next, we have taken 10 snapshots calculated at various time instances by Eq. (40) for the reduced-order model (ROM). We have computed the snapshots at an increased extraction rate of $5 \times 10^4\, m^3/day$ for obtaining a significant response from every part of the aquifer. This has helped us in profoundly identifying the patterns of the system response.

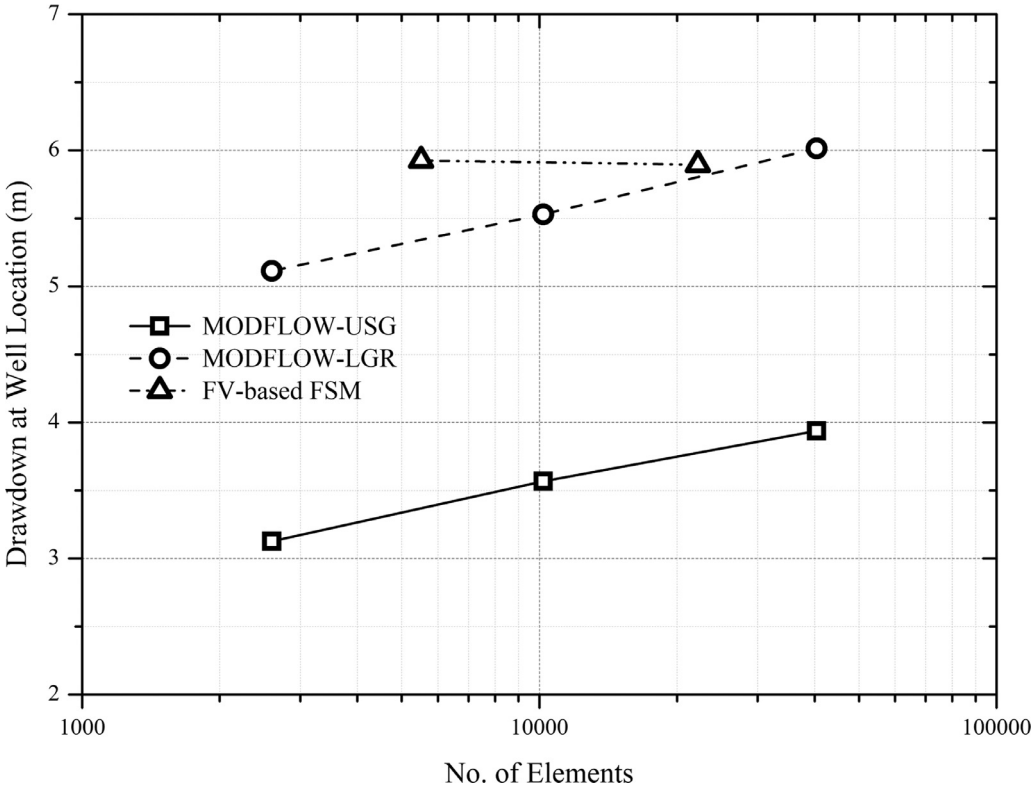

Fig. 6. Comparison of grid-convergence of MODFLOW and FV-based FSM.

Table 1
Comparison of MODFLOW and proposed FV-based FSM results for different grid dimensions.

Simulation Model Used	No. of Elements	Effective Well Radius (m)	Drawdown at well location (m)	CPU Time per iteration
MODFLOW-USG	2601	12.6	3.1267	7.98×10^{-3}
MODFLOW-USG	10201	6.3	3.5672	8.46×10^{-3}
MODFLOW-USG	40401	3.2	3.9376	2.14×10^{-2}
MODFLOW-LGR	2601	0.5	5.1137	1.8×10^{-2}
MODFLOW-LGR	10201	0.25	5.5301	2.18×10^{-2}
MODFLOW-LGR	40401	0.1	6.0148	4.92×10^{-2}
FV-based FSM	5516	0.1	5.9256	2.32×10^{-3}

Table 2
Comparison of error statistic parameter values and CPU computation time for *TC*2, *TC*3 and *TC*4.

Example	Max. AE (m)	MAE (m)	RMSE (m)	NRMSE	CPU Time Reduction (Order)
*TC*2	4.2×10^{-5}	3.7×10^{-6}	4.9×10^{-6}	8.3×10^{-7}	~ 485
*TC*3	4.2×10^{-4}	2.8×10^{-5}	5.4×10^{-5}	1.4×10^{-5}	~ 456
*TC*4	3.6×10^{-3}	2.4×10^{-3}	2.6×10^{-3}	6.4×10^{-4}	~ 610

The POD basis computed from the snapshot matrix comprises 9 vectors. Therefore, for every time step, the ROM needs to solve 9 equations as compared to 5516 by the FSM. As a result, we can ensure a significant reduction in computation time and CPU memory usage. The ROM replicates the FSM with a maximum absolute error of 4.2×10^{-5} m from the entire domain. The other error statistic parameter values tabulated in Table 2 also determine the accuracy of the ROM and justify its applicability as an alternative for the FSM. We have shown the comparison of drawdown contours calculated by the FSM and the ROM after 15 days of constant extraction in Fig. 7. While discretizing the governing equation for all the test problems we have adopted the Crank-Nicholson scheme ($\theta = 0.5$) for temporal averaging.

6.3. TC3: *Transient groundwater flow model with a single extraction well in a heterogeneous confined aquifer*

In *TC*3, we have solved the problem in *TC*2 assuming the confined aquifer to be heterogeneous. We have generated a randomly distributed heterogeneous hydraulic conductivity field based on the field values from 75 sampled locations (*TC*1) following Algorithm 1. We have

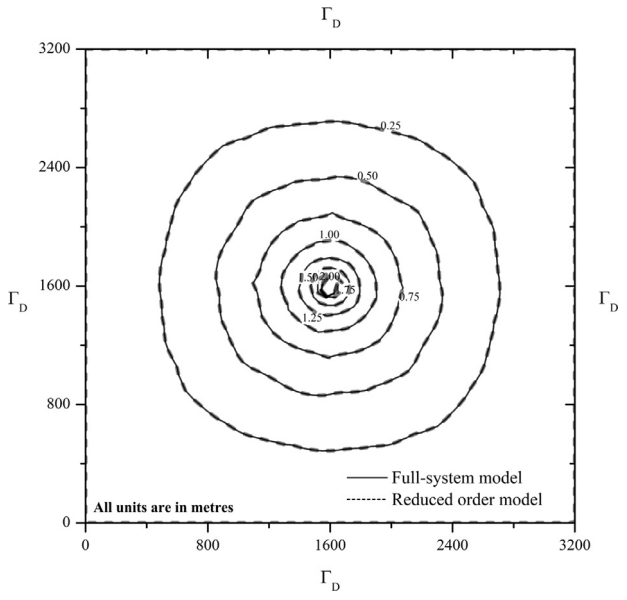

Fig. 7. Comparison of drawdown contours between FSM and ROM after 15 days of extraction for *TC*2.

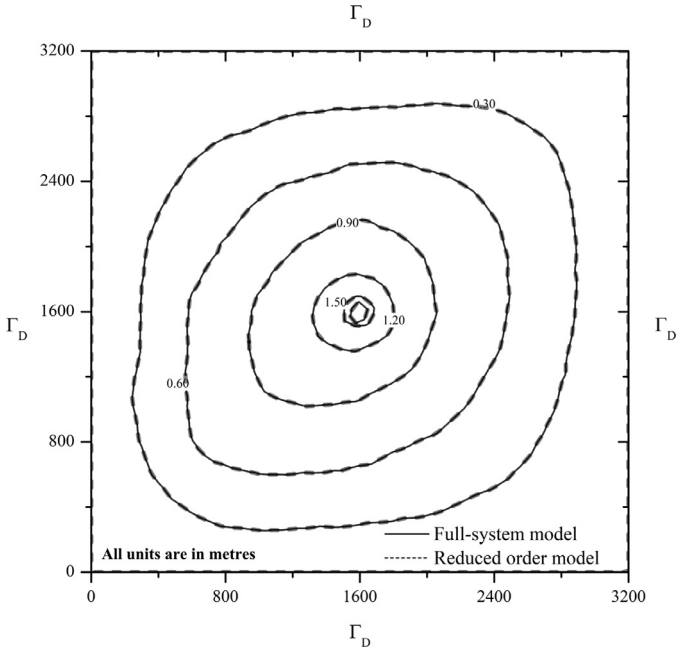

Fig. 8. Comparison of drawdown contours between FSM and ROM after 30 days of extraction for *TC*3.

performed the pumping test for 30 *days*. We have observed the system to attain steady-state conditions approximately within 10 *days* from the commencement of the pumping test (Figure SF2c). Hence, we have captured 20 snapshots of the FSM within that interval for POD basis calculation. Here again, we have calculated the snapshots at an enhanced extraction rate of $5 \times 10^4\, m^3/day$. We have computed a POD basis of 12 vectors from the snapshot matrix. We have presented in Fig. 8 the comparison of drawdown contours at the end of the pumping test for the FSM and the ROM. The results imply that the accuracy of the ROM reduces in replicating the dynamics of the aquifer due to the incorporation of random heterogeneity. The maximum absolute error of estimation has been reduced to $4.2 \times 10^{-4}\, m$ in comparison to *TC*2. We have observed the absolute estimation error to be more in the top right corner and bottom left corner of the field compared to the other parts. Analysing the hydraulic conductivity field, we can infer that the estimation error over the domain is higher in the zones of low hydraulic conductivity (Fig. 10a). However, the plot of absolute nodal error distribution in Fig. 10b shows that the absolute error for more than 90% of the domain has been less than $10^{-4}\, m$. Hence, we can consider the ROM to be capable of reproducing the FSM for a randomly distributed heterogeneous confined aquifer.

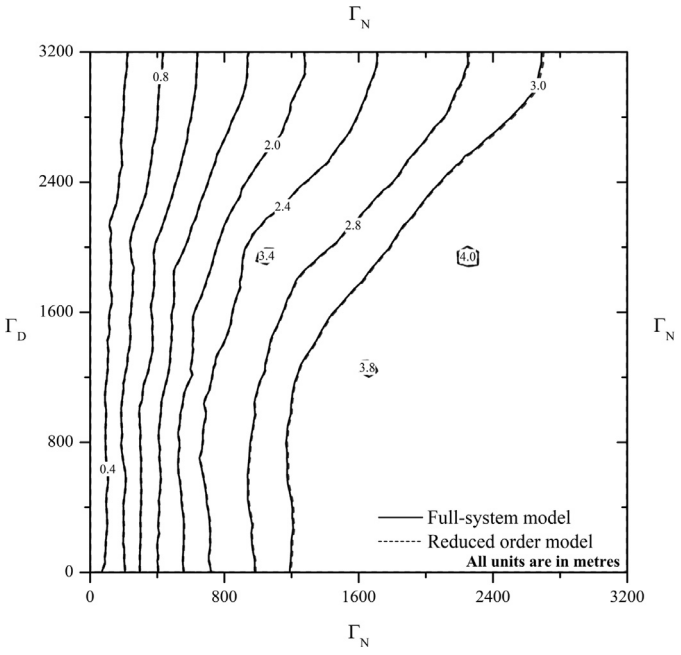

Fig. 9. Comparison of drawdown contours between FSM and ROM after 90 days of extraction for *TC*4.

6.4. TC4: *Transient groundwater flow model with multiple extraction wells in a heterogeneous confined aquifer*

In *TC*4, we have intensified the complexity of the problem by introducing multiple extraction wells and Neumann boundary in the synthetic confined aquifer illustrated in *TC*1. We have considered zero Dirichlet boundary condition on the left boundary of the aquifer, while the other three boundaries are assumed to be impervious. We have assumed the depth of the aquifer to be 100 *m*. Three extraction wells located at (1650,1250), (1050,1950) and (2250,1950) (Figure SF3a) have been operated at a constant rate of $5 \times 10^3\, m^3/day$ throughout the duration of the 90 *days* pumping test. We have discretized the aquifer into 2884 nodes with 5582 triangular elements, and we have generated a randomly distributed heterogeneous hydraulic conductivity field following Algorithm 1 similar to the one conducted in *TC*3. In order to determine the approximate steady state time, we have compared the drawdowns at 6 locations within the domain (Figure SF3a). We have conducted 3 separate runs of the FSM, one extraction well being operated at a time while the others wells remaining inoperative. From Figures SF3b, SF3c and SF3d, we have estimated that the system attains steady-state conditions approximately after 75 *days* of constant extraction.

The snapshot selection strategy, in this case, has been different from the previous two cases as multiple extraction wells are operating simultaneously. Here, we need to record the response of the system separately for each time-invariant and linearly-independent forcing agent. We have captured 75 snapshots of the system dynamics separately for each extraction well, considering it to be extracting at an enhanced rate of $5 \times 10^4\, m^3/day$ while others are inoperative during that time period. We have combined the 3 sets of snapshots to form the final snapshot

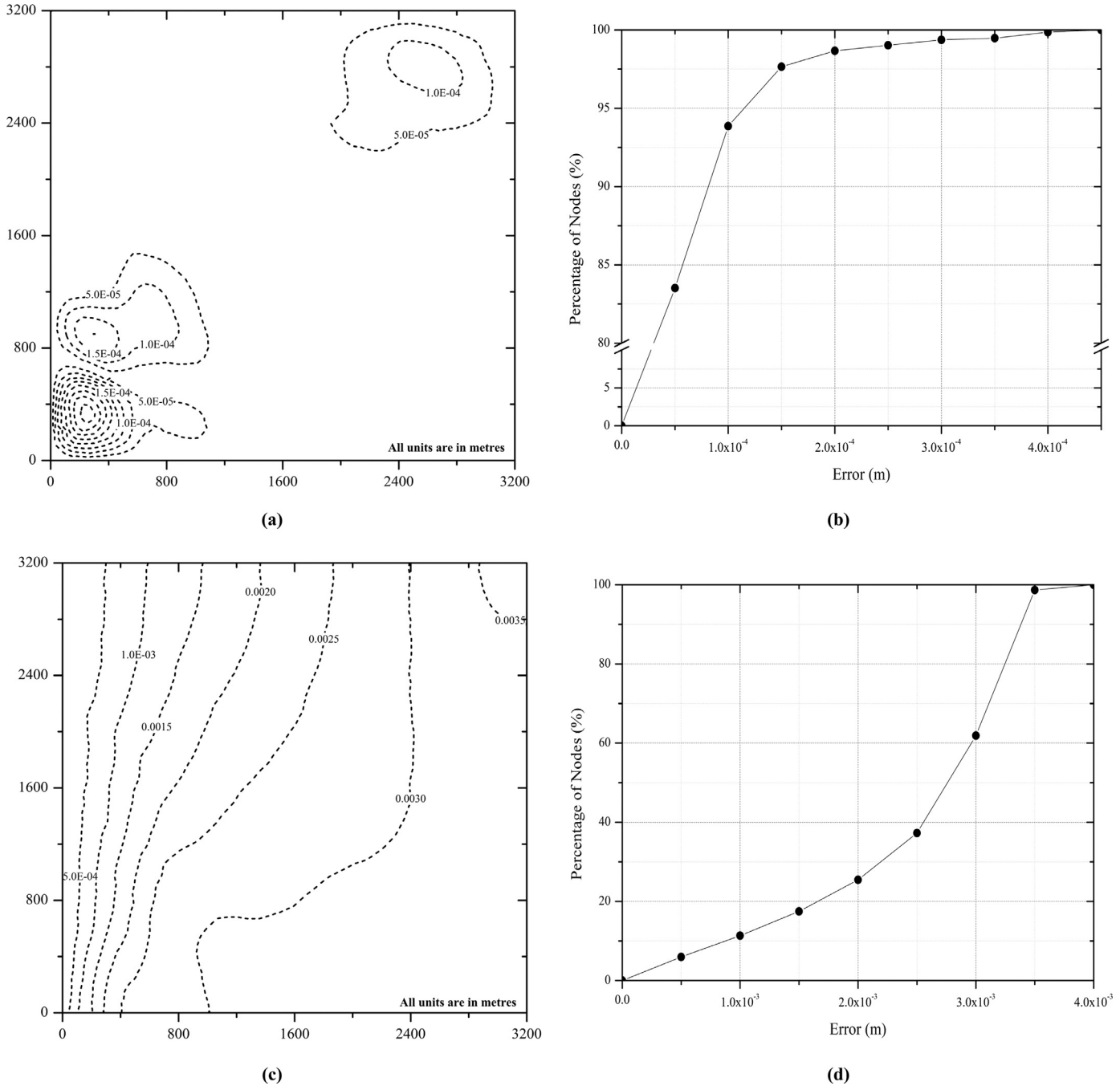

Fig. 10. (a) Contour diagram of absolute drawdown error after 30 days of extraction for *TC*3. (b) Distribution of absolute drawdown error for all nodes of the irregular-unstructured grid of *TC*3. (c) Contour diagram of absolute drawdown error after 90 days of extraction for *TC*4. (d) Distribution of absolute drawdown error for all nodes of the irregular-unstructured grid of *TC*4.

matrix consisting of 225 drawdown vectors. Singular Value Decomposition of the final snapshot matrix identifies 20 principal modes to be dominant that constitute the POD basis. In Fig. 9, we have displayed the comparison of drawdown contours for the FSM and the ROM after 90 days of constant extraction. We have observed that the accuracy of ROM is reducing with the increase in complexity of the boundary conditions as the maximum absolute error has increased to $3.6 \times 10^{-3}\ m$. We have discovered the accuracy of the ROM to be significantly high near the Dirichlet boundary which reduces gradually while moving towards the impervious boundaries (Fig. 10c). In *TC*4 the estimation errors are dominant near the Neumann boundaries, whereas in *TC*3 the low hydraulic conductivity zones primarily account for the errors in estimation. Analyzing the estimation errors for *TC*2, *TC*3 and *TC*4, we can comment that the accuracy of the ROM is affected more by the Neumann boundaries than by the heterogeneity of the conductivity field. The plot of absolute nodal error distribution for *TC*4 (Fig. 10d) reveals that approximately more than 60% of the domain exhibits estimation error less than $3 \times 10^{-3}\ m$, thereby ensuring the application of the proposed ROM for potential replication of the FSM for multiple-well and complex boundary test problems.

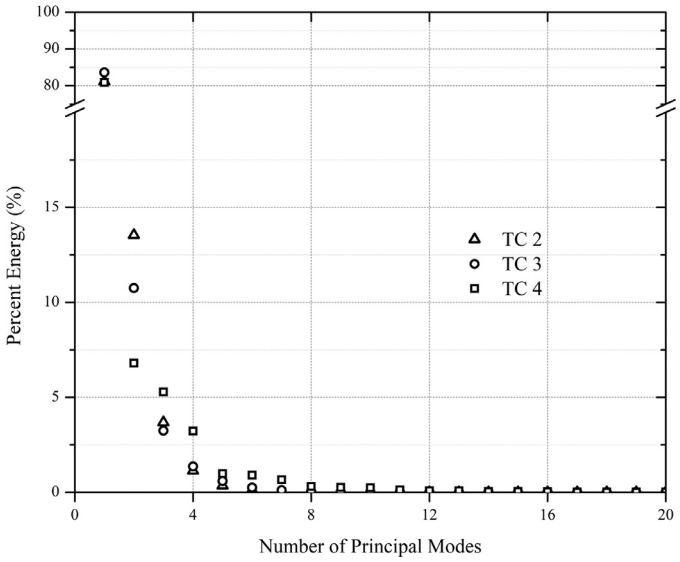

Fig. 11. Comparison of energy percentage from applying SVD for *TC*2, *TC*3 and *TC*4.

7. Summary and conclusions

In this research work, we have presented an algorithm for generating spatially-distributed random hydraulic conductivity fields on an irregular-unstructured grid system based on field values measured from sampled locations within the domain to define aquifers with strong local heterogeneity. We have also presented an irregular-unstructured grid FV formulation for modeling groundwater flow through such randomly heterogeneous confined aquifers with special treatment of singular point source/sink terms. Furthermore, we have developed a model-order reduction methodology based on global POD basis functions for cutting down the computational expenses associated with such full-system groundwater models. The field generation algorithm is not only capable of producing a picture of overall heterogeneity of the domain but also incorporates randomness at a micro-scale level (random hydraulic conductivity value for each element) to define the effects of local heterogeneity. The algorithm generates similar replicates of the heterogeneous field for finer spatial discretization, thereby fulfilling the grid-convergence criteria (Figure SF1). We have observed the results of the FV-based FSM to overcome the issues of grid-convergence faced by MODFLOW-USG using the standard well (WEL) package. The FSM is fast and accurate, and also shows promising convergence results with decreasing grid dimensions for all the test cases (Figures SF4, SF5, SF6). The proposed ROM reproduces the FSM with the desired accuracy for the considered test problems and also shows efficient grid-convergence (Figure SF7). The comparison of the results of the FSM and the ROM suggests that our proposed ROM estimates the drawdowns very accurately in regions of large drawdowns. If the order of calculated responses for a certain considered forcing agent is small, a difficulty arises in pattern identification technique. This can be overcome by considering an increased value of the forcing agent and compute a parameter-independent POD basis for the ROM. However, careful observation reveals that the ROM solutions are most accurate near the extraction well nodes where the system is highly responsive. We have detected somewhat lesser accuracy in the zones of low responses, i.e. the low conductivity regions and also near the boundaries, especially the Neumann boundaries. The key benefit of the proposed ROM lies in its ability to reduce the CPU computation time. Application of POD reduces the high-dimensional solution space to a low-dimensional sub-space consisting of 9, 11 and 20 modes for *TC*2, *TC*3 and *TC*4 respectively, that preserve 99.99% of the total energy. Fig. 11 compares the energy percentage of the dominant modes for the three test cases. For *TC*2 and *TC*3, we have achieved approximately 485 and 456 times reduction in computation time, respectively, with respect to the FSM. Computation time reduction is much more significant for problems with complex boundary conditions. This has been evident in *TC*4, where we have achieved a greater time reduction of approximately 610 times through the ROM. However, computation time reduction has increased significantly while reproducing the previous problems with finer spatial discretization (Table ST1). Besides, we have also accomplished a significant reduction of CPU storage as we have solved the governing equation in a reduced sub-space with the same set of POD basis for every time iteration.

The primary objective of this study is to verify the proposed methodologies of random hydraulic conductivity field generation and computationally inexpensive groundwater modeling on theoretical aquifer systems. The results confirm that the above methodologies are likely to be applied for natural aquifer systems on catchment-scale. Groundwater dynamics of a catchment comprising a confined aquifer can be characterized applying the proposed methodologies. To begin with, the field hydraulic conductivity values need to be measured through field-tests from priorly designated sample locations over the catchment. Next, a mean-hydraulic conductivity field for the catchment can be generated using Algorithm 1 on a regular or an irregular-unstructured grid system depending on the catchment geometry. Finally, with proper information about the catchment boundaries and available hydrological data, the proposed ROM can simulate the groundwater head distribution over the catchment. In conclusion, the performance evaluation of the proposed FV-based full-system groundwater model and corresponding reduced-order model prove their potential applicability at estimating groundwater dynamics for both homogeneous and heterogeneous confined aquifer systems, subjected to variable boundary conditions and multiple forcing agents. We plan on extending the methodology to solve flow problems involving non-linearity and unfurl the applicability of the proposed methods to solve groundwater flow problems through unconfined and coastal aquifers.

Notations

- $\mathbf{A}$ = Stiffness matrix.
- A_f = Surface area of the element boundary. $[L^2]$
- A_α, A_β = Voronoi polygon area corresponding to sampled locations and area of an element of the irregular-unstructured grid respectively. $[L^2]$
- b = Depth of the confined aquifer. $[L]$
- C_z = Covariance function.
- c = Power-law constant.
- d_1, d_2 = Distance of the center of an element face respectively from the centroid of the parent element, and the neighbor element adjacent to that face. $[L]$
- $\mathbf{f}$ = Force vector.
- H_0 = Static hydraulic head. $[L]$
- $\mathbf{I_f}$ = Vector directed from the centroid of the parent element to the centroid of the neighbor element adjacent to the face f.
- $\mathbf{K}$ = Hydraulic conductivity tensor.
- K_f = Face-centered hydraulic conductivity of the f^{th} face of the element. $[LT^{-1}]$
- K_x, K_y = Hydraulic conductivity in X and Y directions respectively. $[LT^{-1}]$
- K_α, $K_\beta{}^*$ = Field hydraulic conductivity at sampled locations and estimated hydraulic conductivity for irregular-unstructured grid elements respectively. $[LT^{-1}]$
- L = Estimation error variance function.
- L_f = Length of the face f of an element. $[L]$
- M_c = Number of Monte Carlo realizations.
- m = Mean of the sampled field hydraulic conductivity values.
- m_c, m_{uc} = Conditional and unconditional means respectively.

- m_{uca}, $m_{uc\beta}$ = Mean of the primary and secondary basis values respectively within the defined respective neighborhood of an element.
- m_1, m_2 = Number of primary and secondary basis points respectively within the defined neighborhood of an element.
- $m_{1\max}$, $m_{2\max}$ = Maximum number of primary and secondary basis points to be considered within the defined neighborhood of an element respectively.
- $N_{c\min}$ = Minimum number of conditioning values to be considered for an element.
- N_r = A random integer.
- N_s = Specific volumetric point source/sink. $[T^{-1}]$
- n_{e1}, n_{e2}, n_{e3} = Number of elements associated with first, second and third node of an element respectively.
- n_p = Number of elements associated with any node.
- $\tilde{n_p}$ = Number of principal components.
- n_{set} = Number of sets of snapshots.
- $n_{\tilde{t_s}}$ = Number of snapshots in each set.
- $\hat{\mathbf{n}}$ = Normal vector at the boundary.
- $\hat{\mathbf{n_f}}$ = Unit vector in the outward normal direction from the point of intersection of the line joining the centroids of the parent and the adjacent neighbor element on the face *f*.
- n_1, n_2 = Number of sampled locations and number of elements in the irregular-unstructured grid respectively.
- $\mathbf{P}$ = POD basis matrix.
- Q_p = Volumetric extraction rate of the extraction well. $[L^3T^{-1}]$
- q_N = A known function.
- r = Distance of the extraction well node from the centroid of the element associated to it. $[L]$
- $\mathbf{r_n}$ = Time-dependent coefficient vector.
- r_w = Radius of the extraction well. $[L]$
- S = Storage Coefficient.
- S_s = Specific storage of the confined aquifer. $[L^{-1}]$
- $\mathbf{S_{snap}}$ = Snapshot matrix.
- s_a = Drawdown. $[L]$
- $\tilde{\mathbf{s_a}}$ = Estimated drawdown vector.
- s_{aD}, s_{a0} = Known functions.
- T_f = Face-centered transmissivity of the f^{th} face of the element. $[L^2T^{-1}]$
- T_{final} = Final extraction time.
- $\tilde{T_s}$ = Approximate steady state time.
- t = Time coordinate.
- $\hat{\mathbf{t_f}}$ = Unit vector in the tangential direction along face *f* from the point of intersection of the line joining the centroids of the parent and the adjacent neighbor element.
- $\tilde{\mathbf{t_s}}$ = Snapshot time-set.
- $\mathbf{U}$, $\mathbf{V}$ = Matrix of left and right singular vectors respectively.
- W_s = Specific volumetric source or sink. $[T^{-1}]$
- w_f, w_n = Element to face inverse distance-weighted interpolation function and Element to node area-weighted interpolation function respectively.
- $\mathbf{x}$ = Vector of space coordinates in the Euclidean space. $[L]$
- Z_α, $Z_\beta{}^*$ = Natural logarithmic value of field hydraulic conductivity at sampled locations and estimated logarithmic value of hydraulic conductivity for irregular-unstructured grid elements respectively. $[LT^{-1}]$
- z_a = Hydraulic head. $[L]$
- Γ_D, Γ_N = Dirichlet and Neumann boundaries respectively.
- γ = Model semivariogram.
- δ = Dirac Delta function.
- δ_{nf}, δ_{tf} = Distance between the centroids of the parent element and neighbor element adjacent to the face *f* in the normal and tangential directions to the face respectively. $[L]$
- ϵ_R = Incremental value of R_1 for each iteration. $[L]$
- θ = Degree of implicitness.
- λ_α, λ_β = Kriging coefficient corresponding to primary and secondary basis values respectively.
- μ = Lagrange multiplier.
- $\mathbf{\Sigma}$ = Diagonal matrix with the singular values as the diagonal elements.
- σ = Singular value.
- $\sigma_c{}^2$, $\sigma_{uc}{}^2$ = Conditional and unconditional variances respectively.
- $\sigma_{error}{}^2$ = Estimation error variance.
- ϕ_α, ϕ_β = Area-weighting coefficient corresponding to primary and secondary basis values respectively.
- Ω = Physical Domain.
- ω = Power-law exponent.
- φ = Angle subtended in radians with the extraction well node by the element associated to it.
- $\mathcal{F}$ = Inward flux from the associated element to the extraction well node. $[L^3T^{-1}]$

Declaration of Competing Interest

The authors declare that they have no known competing financial interests or personal relationships that could have appeared to influence the work reported in this paper.

Supplementary material

Supplementary material associated with this article can be found, in the online version, at doi:10.1016/j.advwatres.2020.103703.

CRediT authorship contribution statement

Saumava Dey: Conceptualization, Methodology, Validation, Writing - original draft. **Anirban Dhar:** Supervision, Writing - review & editing.

References

Ababou, R., 1988. Three-dimensional flow in random porous media. Massachusetts Institute of Technology, Cambridge, Massachusetts.

Abbaszadeh, M., Dehghan, M., 2020. An upwind local radial basis functions-differential quadrature (RBFs-DQ) technique to simulate some models arising in water sciences. Ocean Eng. 197.

Adler, P.M., Thovert, J.F., 1993. Fractal porous media. Transp. Porous Media 13 (1), 41–78.

Baú, D.A., 2012. Planning of groundwater supply systems subject to uncertainty using stochastic flow reduced models and multi-objective evolutionary optimization. Water Resour. Manage. 26 (9), 2513–2536.

Bear, J., 1979. Hydraulics of Groundwater. McGraw-Hill International Book Co., New York.

Bellin, A., Rubin, Y., 1996. HYDRO_GEN: a spatially distributed random field generator for correlated properties. Stochas. Hydrol. Hydraul. 10 (4), 253–278.

Bergström, D., Powell, J., Kaplan, A.F.H., 2007. A ray-tracing analysis of the absorption of light by smooth and rough metal surfaces. J Appl Phys 101 (11).

Boyce, S.E., Nishikawa, T., Yeh, W.W.-G., 2015. Reduced order modeling of the Newton formulation of MODFLOW to solve unconfined groundwater flow. Adv. Water Resour. 83, 250–262.

Boyce, S.E., Yeh, W.W.-G., 2014. Parameter-independent model reduction of transient groundwater flow models: application to inverse problems. Adv Water Resour 69, 168–180.

Chen, Z., Zhang, Y., 2009. Well flow models for various numerical methods.. Int. J. Numer. Anal. Model. 6 (3), 375–388.

Clifton, P.M., Neuman, S.P., 1982. Effects of kriging and inverse modeling on conditional simulation of the Avra Valley aquifer in Southern Arizona. Water Resour. Res. 18 (4), 1215–1234.

Dagan, G., 1982. Stochastic modeling of groundwater flow by unconditional and conditional probabilities: 1. conditional simulation and the direct problem. Water Resour. Res. 18 (4), 813–833.

Dehghan, M., Abbaszadeh, M., 2018. The solution of nonlinear Green-Naghdi equation arising in water sciences via a meshless method which combines moving kriging interpolation shape functions with the weighted essentially nonoscillatory method. Commun. Nonlinear Sci. Numer. Simul. 68, 220–239.

Delhomme, J.P., 1979. Spatial variability and uncertainty in groundwater flow parameters: a geostatistical approach. Water Resour. Res. 15 (2), 269–280.

Diersch, H.-J.G., 2014. FEFLOW Finite Element Modeling of Flow, Mass and Heat Transport in Porous and Fractured Media. Springer.

Dotlić, M., Vidović, D., Pokorni, B., Pušić, M., Dimkić, M., 2016. Second-order accurate finite volume method for well-driven flows. J. Comput. Phys. 307, 460–475.

Emery, X., Lantuéjoul, C., 2006. TBSIM: a computer program for conditional simulation of three-dimensional gaussian random fields via the turning bands method. Comput. Geosci. 32 (10), 1615–1628.

Freeze, R.A., 1975. A stochastic-conceptual analysis of one-dimensional groundwater flow in nonuniform homogeneous media. Water Resour Res 11 (5), 725–741.
Goovaerts, P., 1997. Geostatistics for Natural Resources Evaluation. Oxford University Press.
Greenkorn, R.A., Kessler, D.P., 1969. Dispersion in heterogeneous nonuniform anisotropic porous media. Ind. Eng. Chem. 61 (9), 14–32.
Haasdonk, B., Ohlberger, M., 2011. Efficient reduced models and a posteriori error estimation for parametrized dynamical systems by offline/online decomposition. Math. Comput. Model. Dyn. Syst. 17 (2), 145–161.
Harbaugh, A.W., 2005. MODFLOW-2005, The U.S. Geological Survey Modular Ground-Water Modelthe Ground-Water Flow Process. U.S. Geological Survey.
Harbaugh, A.W., Banta, E.R., Hill, M.C., McDonald, M.G., 2000. MODFLOW-2000, the U.S. Geological Survey modular ground-water model user guide to modularization concepts and the ground-water flow process. Open-File Report 00-92.
Hasenauer, J., Löhning, M., Khammash, M., Allgöwer, F., 2012. Dynamical optimization using reduced order models: a method to guarantee performance. J. Process Control 22 (8), 1490–1501.
Ilati, M., Dehghan, M., 2016. Remediation of contaminated groundwater by meshless local weak forms. Comput. Math. Applic. 72 (9), 2408–2416.
Isaaks, E.H., Srivastava, R.M., 1989. An Introduction to Applied Geostatistics. Oxford University Press.
Kani, J.N., Elsheikh, A.H., 2019. Reduced-order modeling of subsurface multi-phase flow models using deep residual recurrent neural networks. Transp. Porous Media 126, 713–741.
Kobayashi, S., Nishimura, N., 1992. Boundary Element Methods Fundamentals and Applications. Springer.
Leveque, R.J., 2002. Finite Volume Methods for Hyperbolic Problems. Cambridge University Press, Cambridge.
Lin, G.-F., Chen, G.-R., 2005. Quantifying uncertainty of the semivariogram of transmissivity of an existing groundwater monitoring network. Hydrol. Process 19 (10), 2023–2034.
Liu, G.R., Gu, Y.T., 2005. An Introduction to Meshfree Methods and Their Programming. Springer.
Loudyi, D., Falconer, R.A., Lin, B., 2006. Mathematical development and verification of a non-orthogonal finite volume model for groundwater flow applications. Adv. Water Resour. 30 (1), 29–42.
Mazumder, S., 2016. Numerical Methods For Partial Differential Equations Finite Difference and Finite Volume Methods. Elsevier.
McDonald, M.G., Harbaugh, A.W., 1988. A Modular Three-dimensional Finite-difference Ground-water Flow Model. U.S. Geological Survey.
McPhee, J., Yeh, W.W.-G., 2008. Groundwater management using model reduction via empirical orthogonal functions. J. Water Resour. Plann. Manage. 134 (2), 161–170.
Mehl, S., Hill, M.C., 2002. Development and evaluation of a local grid refinement method for block-centered finite-difference groundwater models using shared nodes. Adv. Water Resour. 25 (5), 497–511.
Narasimhan, T.N., Witherspoon, P.A., 1976. An integrated finite difference method for analyzing fluid flow in porous media. Water Resour Res 12 (1), 57–64.
Panday, S., Langevin, C.D., Niswonger, R.G., Ibaraki, M., Hughes, J.D., 2013. MODFLOWUSG version 1: an unstructured grid version of MODFLOW for simulating groundwater flow and tightly coupled processes using a control volume finite-difference formulation. Techniques and Methods 6-A45.
Papadopulos, I.S., Cooper, H.H., 1967. Drawdown in a well of large diameter. Water Resour. Res. 3 (1), 241–244.
Park, H.M., Cho, D.H., 1996. Low dimensional modeling of flow reactors. Int J Heat Mass Transf 39 (16), 3311–3323.
Park, H.M., Chung, O.Y., Lee, J.H., 1999. On the solution of inverse heat transfer problem using the Karhunen–Loeve Galerkin method. Int. J. Heat Mass Transf. 42 (1), 127–142.
Pasetto, D., Guadagnini, A., Putti, M., 2011. POD-based Monte Carlo approach for the solution of regional scale groundwater flow driven by randomly distributed recharge. Adv. Water Resour. 34 (11), 1450–1463.
Pasetto, D., Putti, M., Yeh, W.W.-G., 2013. A reduced-order model for groundwater flow equation with random hydraulic conductivity: application to Monte Carlo methods. Water Resour. Res. 49 (6), 3215–3228.
Peaceman, D.W., 1977. Interpretation of well-block pressures in numerical reservoir simulation. Soc. Petrol. Eng. J. 18 (3).
Peaceman, D.W., 1983. Interpretation of well-block pressures in numerical reservoir simulation with nonsquare grid blocks and anisotropic permeability. Soc. Petrol. Eng. J. 23 (3).
Pinder, G.F., Celia, M.A., 2006. Subsurface Hydrology. John Wiley & Sons, New Jersey.
Reddy, J.N., 2006. Introduction to the Finite Element Method. McGraw-Hill Education.
Remy, N., Boucher, A., Wu, J., 2009. Applied Geostatistics with SGeMS: A Users Guide. Cambridge University Press.
Rogiers, B., Mallants, D., Batelaa, O., Gedeon, M., Huysmans, M., Dassargues, A., 2012. Estimation of hydraulic conductivity and its uncertainty from grain-size data using GLUE and artificial neural networks. Math. Geosci. 44 (6), 739–763.
Sahimi, M., Yortsos, Y.C., 1990. Applications of Fractal Geometry to Porous Media: A Review. Society of Petroleum Engineers Publication, p. 20476.
Siade, A.J., Putti, M., Yeh, W.W.-G., 2010. Snapshot selection for groundwater model reduction using proper orthogonal decomposition. Water Resour. Res. 46 (8).
Sirovich, L., 1987. Turbulence and the dynamics of coherent structures. i. coherent structures. Q. Appl. Math. 45 (3), 561–571.
Smith, I.M., Griffiths, D.V., Margetts, L., 2013. Programming the Finite Element Method. Wiley, New York.
Stanko, Z.P., Boyce, S.E., Yeh, W.W.-G., 2016. Nonlinear model reduction of unconfined groundwater flow using POD and DEIM. Adv. Water Resour. 97, 130–143.
Thiem, G., 1906. Hydrologische Methoden. Gebhardt, Leipzig, Germany.
Tsai, F.T.-C., 2006. Enhancing random heterogeneity representation by mixing the kriging method with the zonation structure. Water Resour. Res. 42 (W08428).
Vermeulen, P.T.M., Heemink, A.W., Stroet, C.B.M.T., 2004. Low-dimensional modelling of numerical groundwater flow. Hydrol. Process. 18 (8), 1487–1504.
Xu, Z., Wang, X., Chai, J., Qin, Y., Li, Y., 2017. Simulation of the spatial distribution of hydraulic conductivity in porous media through different methods. Math. Probl. Eng..
Yeh, W.W.-G., 1986. Review of parameter identification procedures in groundwater hydrology: the inverse problem. Water Resour. Res. 22 (2), 95–108.
Yu, Y.X., Wu, J.C., 2006. Application of electrical resistivity tomography data to estimate hydraulic conductivity in porous medium. Hydrogeol. Eng. Geol. 33 (2), 41–44.
Lin, J., Richards, D., Talbot, C., Yeh, G.-T., Cheng, R., Cheng, H.-P., Jones, N., 1997. FEMWATER: A Three-Dimensional Finite Element Computer Model for Simulating Density-Dependent Flow and Transport in Variably Saturated Media. US Army Corps of Engineers: Waterways Experiment Station, Technical Report CHL-97-12.